Improvement of the linearly polarized output power in Nd:YAG laser with [100]-cut rod

Zhe Sun (孙 哲)*, Qiang Li (李 强), Menghua Jiang (姜梦华), Hong Lei (雷 訇), and Yongling Hui (惠勇凌)

Institute of Laser Engineering, Beijing University of Technology, Beijing 100124, China

**Corresponding author: allen-sun@emails.bjut.edu.cn*

Received August 5, 2011; accepted October 24, 2011; posted online April 18, 2012

Thermal depolarization caused by birefringence is a major factor that limits the output power of linearly polarized Nd:YAG laser. This paper theoretically analyzes the thermal depolarization of [111]- and [100]-cut Nd:YAG rods and output power of two diode-pumped Nd:YAG rods are compared experimentally. ϕ3×80 mm sized [111]- and [100]- cut rods with doping concentration of 1.1±0.1at.% are used. With a pump power of 180 W, the ratio of linearly polarized output power versus unpolarized output power obtained with the [111]- and [100]- cut rods are 19% and 43% respectively, with a difference of 24%. The experiment demonstrates that in comparison with conventional [111]- cut Nd:YAG rod, [100]- cut Nd:YAG rod can improve the linearly polarized output power obviously. The thermal depolarization depends on the polarization direction for the [100]- cut Nd:YAG rod, and the linearly polarized output power can be improved by suitably modification of the polarization direction of linearly polarized laser to minimize thermal depolarization.

OCIS codes: 140.3530, 140.3538, 140.6810.

doi: 10.3788/COL201210.S11402.

Diode-pumped solid-state laser has grown dramatically in recent years. The main problem restricting solid-state laser power is unavoidable heat release in active elements due to pump absorption[1,2]. Thermal effects induced stress birefringence changes in refractive index, strain and even destruction of active element that all affect the quality of a beam propagating through the crystal in solid state lasers[3,4]. It results in depolarization of a linearly polarized beam, since the refractivity power of the thermally induced birefringence depends on the polarization direction, which limits the output power of linearly polarized Nd:YAG lasers[5].

There were a number of techniques to reduce the birefringence. The majority of the techniques involve the insertion of various types of components like Faraday rotator[6,7], optical rotator[8,9] or wave plate[10–12] into the resonator cavity to compensate the birefringence. But these approaches have resulted in additional loss and more complex design, which can only reduce depolarization loss below 5%. A simply potential method to reduce depolarization in Nd:YAG rod laser has been presented, which is to replace the conventional [111]-cut with other cut directions[13,14]. The theoretical analysis of depolarization induced by birefringence in Nd:YAG crystal was investigated[15–17]. The depolarization of [100]-cut Nd:YAG was measured by a single pass probe beam[18]. However, the presented experiment with probe beam didn't intrinsically reveal the depolarization loss for laser operation, since the Nd:YAG rod is passed more than once in reality.

In this letter, we present the experimental research of laser diode (LD) side pumped [111]- and [100]-cut Nd:YAG rods which are based on theoretical analysis. The result demonstrates that depolarization depends on the polarization direction of [100]-cut rod, and it can actually reduce the depolarization loss compared with [111]-cut rod with suitably modification of the polarization direction. Using the [100]-cut Nd:YAG rod as the laser medium can improve the linearly polarized output power for laser operation.

As a cubic crystal, YAG is optically isotropic and its optical indicatrix is a sphere. The [111]-cut is the conventional cutting direction for Nd:YAG crystal. The [100]-cut Nd:YAG crystal orientation for the cylindrical symmetry are shown in Fig. 1. The crystal lattice is shown in Fig. 1(a), the x axis is in the [001]-direction, the y axis is in the [010]-direction and the z axis is in the [100]-direction. As shown in Fig. 1(b), Nd:YAG rod is grown with the cylindrical axis along the [100]-direction, and the laser propagates in this direction.

In a Nd:YAG rod, the indicatrix becomes an ellipsoid under thermal stress. In a cylindrical coordinate system, the thermally induced birefringence of [111]- and [100]-cut Nd:YAG crystals orientation were given by[15]

$$(n_{y^*} - n_{x^*}) = \frac{n_0^2}{2}(\varepsilon_r - \varepsilon_\varphi)(p_{11} - p_{12} + 4p_{44}) \quad [111], \tag{1}$$

$$(n_{y^*} - n_{x^*}) = \frac{n_0^2}{2} \cdot \sqrt{(\varepsilon_r - \varepsilon_\varphi)^2[(p_{11} - p_{12})^2 \cos^2 2\varphi + 4p_{44}^2 \sin^2 2\varphi]} \quad [100], \tag{2}$$

where φ is the angle from the y axis.

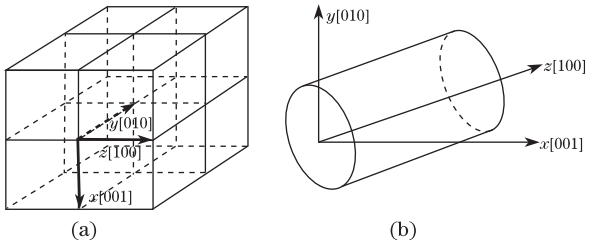

Fig. 1. Crystal orientation for the [100]-cut Nd:YAG rod.

It becomes anisotropic when an optically isotropic material is subject to mechanical stresses. The change of the refractive index is called the stress birefringence or the elasto-optical effect. The state of stress or strain in a material is characterized by the stress tensor σ_{kl} and the strain tensor $\varepsilon_{kl}(k, l{=}1, 2, 3)$. These tensors and the elasto-optical coefficients p_{nm} $(m, n{=}1, 2, 3, 4, 5, 6)$ are different from the dielectric tensor, which determines the optical properties. For Nd:YAG crystal, the approximate values of the elasto-optical coefficients are givenby $p_{11} = -0.0290$, $p_{12}{=}0.0091$, and $p_{44} = -0.0615$[1]. $(\varepsilon_\gamma - \varepsilon_\varphi)$ is given by Koechner et. al.[15] in Eq. (3).

$$(\varepsilon_r - \varepsilon_\varphi) = -2\frac{\alpha A_0}{(1-\nu)16\pi KL}(\nu+1)\frac{r^2}{r_0^2}, \qquad (3)$$

where, r_0 is the rod radius, α is the linear expansion coefficient, A_0 is in watts per cubic centimeter, ν is the Poisson ratio, K is the thermal conductivity, L is the rod length.

To simulate the difference of birefringence between [111]- and [100]-cut Nd:YAG rods, we calculated the birefringence on cross section of the two rods in Fig. 2. The different colors represent the magnitude of birefringence. The blue represents the minimum birefringence and the red represents the maximum birefringence. Axes of refractive index ellipse are in the radial and tangential directions for the [111]-cut Nd:YAG rod under the thermal stress. As Fig. 2(a) shows, the magnitude of birefringence is minimum in the rod center and increases with the increase of distance from the rod center. The distribution of birefringence shows a circle pattern. The birefringence of the [111]-cut rod is always the same in any directions with the same radius. In the same condition, axes of refractive index ellipse are not always in radial and tangential directions for the [100]-cut Nd:YAG rod. As Fig. 2(b) shows, the magnitude of birefringence is minimum in the rod center and the distribution of birefringence shows a crisscross pattern. The birefringence of the [100]-cut rod in transverse and longitudinal direction is obviously smaller than other directions with the same radius. Consequently, the magnitude of birefringence on the cross section of the [100]-cut rod is obviously smaller than that of the [111]-cut rod.

In order to analyze the orientation of the birefringence, the polarization vector of rod cross-section needs to be considered. The principal axes of thermal induced stress birefringence are x^* and y^* axis. The magnitude of birefringence is in proportion to square of radius. The birefringence imposes a depolarization on linearly polarized laser passing through the rod.

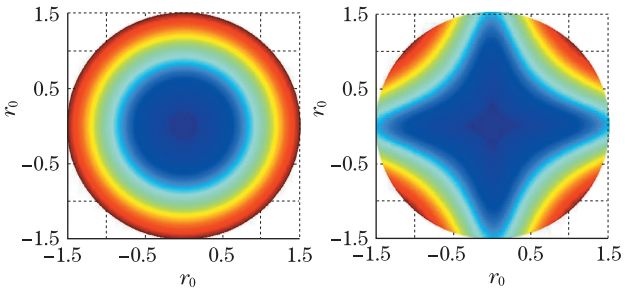

Fig. 2. Simulated birefringence patterns on the cross section of [111]- and [100]-cut Nd:YAG rods.

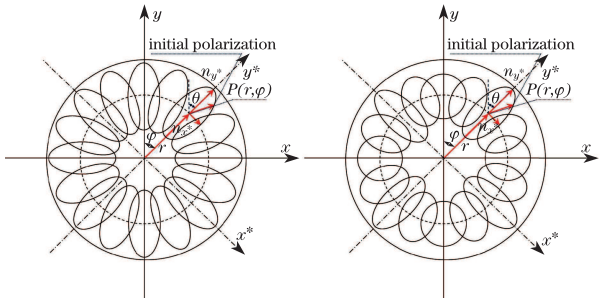

Fig. 3. Schematics of the birefringence on the cross section of the [111]- and [100]-cut Nd:YAG rods when $\varphi = \pi/4$.

For [111]-cut rod, a schematic of cylindrical symmetry of the birefringence is shown in Fig. 3(a). The polarization vector of linearly polarized incident laser is divided into radial and tangential component at point P(r, φ) on the rod. The refractive index for the radially polarized component is n_{y*}. The direction of n_{y*} is always along the radial direction. The refractive index for the tangentially polarized component is n_{x*}. The direction of n_{x*} is perpendicular to n_{y*}. The refractive index n_{x*} and n_{y*} are for the linearly polarized laser along x^* and y^* axis, respectively. Considering that $n_{x*} \neq n_{y*}$, there is a phase difference between the two components as the beam leaves the rod, and the once linearly polarized laser is now elliptically polarized[6]. θ indicates the angle between y axis and n_{y*}. The lattice structure is symmetric about the axis of the rod, thus θ is equal to φ. The relationship between θ and φ for the [111]-cut rod can be expressed as[14]

$$\tan(2\theta) = \tan(2\varphi) \quad [111], \qquad (4)$$

where θ is always equal to φ.

For the [100]-cut rod, the direction of n_{x*} and n_{y*} will not always in the tangential and radial direction. Thus θ is different from φ. The relationship between θ and φ for the [100]-cut rod can be expressed as[14]

$$\tan(2\theta) = \frac{2p_{44}}{p_{11}-p_{12}}\tan(2\varphi) \quad [100]. \qquad (5)$$

Obviously, θ is not always equal to φ in Eq. (5). So the birefringence changes in different polarization directions. The position of maximum and minimum birefringence can be found on the cross section of the [100]-cut rod. The schematic of the birefringence on the cross section of the [100]-cut rod when $\varphi = \pi/4$ is shown in Fig. 3(b). The direction of n_{x*} and n_{y*} in the tangential and radial direction, and the magnitude of n_{y*} is larger than the magnitude of n_{x*} for the [100]-cut rod when $\varphi = \pi/4$. The magnitude of birefringence is maximum in this direction. This conclusion is in good agreement with the simulation of birefringence in Fig. 2.

Theoretical analysis[14,17–19] shows that the minimum depolarization loss can be found through suitably modification of the polarization direction, which is much smaller than that of the [111]-cut Nd:YAG rod. Depolarization is defined as the ratio of the depolarized power to the initial linearly polarized power. The amount of depolarization is represented by[13]

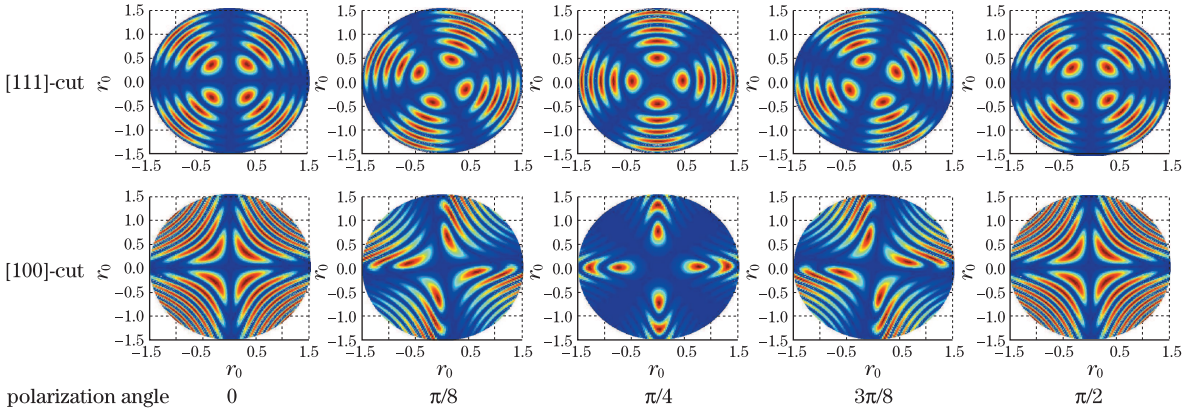

Fig. 4. Simulated depolarization patterns of the cross section of the [100]- and [111]-cut Nd:YAG rods.

$$D_{\rm pol} = \frac{1}{\pi r_0^2}\int_0^{2\pi}\int_{r=0}^{r_0} D r {\rm d}r{\rm d}\varphi, \tag{6}$$

which is the integration of the depolarization.

$$D = \sin^2[2(\theta-\gamma)]\sin^2\left(\frac{\delta}{2}\right) = \sin^2[2(\theta-\gamma)]\sin^2\left(\frac{\pi}{\lambda}L\Delta n\right)$$
$$= \sin^2[2(\theta-\gamma)]\sin^2[\frac{\pi}{\lambda}\Omega\frac{\alpha\eta P_{\rm in}}{(1-\nu)16\pi K}\frac{r^2}{r_0^2}], \tag{7}$$

where δ is the phase difference which is given by the thermally induced birefringence Δn. γ represents the angle between y axis and the direction of the initial polarization direction, λ is the laser wavelength, $P_{\rm in}$ is the absorbed pump power, and η is the fractional thermal loading. Ω for the [111]- and [100]-cut are given by[14]

$$\Omega = \frac{1}{3}n_0^3(1+\nu)(p_{11}-p_{12}+4p_{44}) \quad [111], \tag{8}$$

$$\Omega = n_0^3(1+\nu)[(p_{11}-p_{12})^2\cos^2(2\varphi) - 2p_{44}^2\sin^2(2\varphi)]^{\frac{1}{2}} \quad [100]. \tag{9}$$

Equation (7) contains two parts. The first part "$\sin^2[2(\theta-\gamma)]$" is connect with γ and θ, the second part "$\sin^2\{\Omega\pi\alpha\eta P_{\rm in}r^2/[16\pi(1-\nu)\lambda K r_0^2]\}$" is connect with Ω for both rods. For the [111]-cut rod, Ω is a definite value in Eq. (8). The magnitude of depolarization does not change with the different polarization angle γ. For the [100]- cut rod, Ω changes with different φ in Eq. (9) and φ is also different from θ in Eq. (5). So the magnitude of depolarization changes with the different polarization angle γ.

To quantificationally compare the overall depolarization across the [111]- and [100]-cut Nd:YAG rods, we calculated the depolarization distributions of the both rods for different polarization directions of linearly polarized laser. At a pump power of 180 W and beam radius equal to the rod radius, the depolarization patterns of the cross section of the [111]- and [100]-cut Nd:YAG rods are shown in Fig. 4. The different colors represent the magnitude of depolarization. The blue represents the minimum depolarization and the red represents the maximum depolarization. The pattern of depolarization distribution of the [111]-cut rod rotates accordingly rather than changes with the different polarization directions. However, the pattern of depolarization distribution depends on the polarization direction for the [100]-cut rod. Although the maximum depolarization has been found for angle γ=0 and $\pi/2$, the minimum depolarization has been found for angle $\gamma = \pi/4$ which is obviously smaller than that of the [111]-cut rod. The distribution of depolarization periodically changes as a period of $\pi/2$. It can be found that the overall depolarization from the [100]-cut rod with the polarization angle γ=0 and $\pi/2$ is about 3.2 times of that from the [100]-cut rod with the polarization angle $\gamma = \pi/4$. And the overall depolarization loss from the [111]-cut rod is about 2 times of that from the [100]-cut rod with the polarization angle $\gamma = \pi/4$.

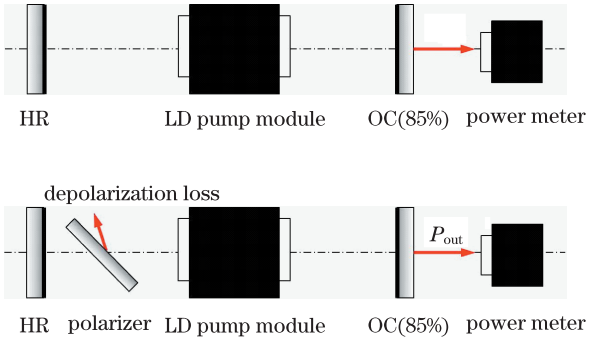

Fig. 5. Schematic of the experiment. (a) Without polarizer; (b) with polarizer.

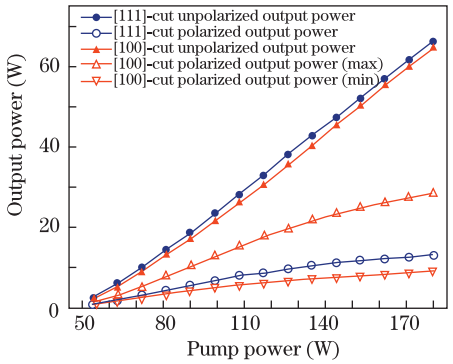

Fig. 6. Output power of polarized and unpolarized laser of the [111]- and [100]-cut Nd:YAG rods with different pump powesrs.

To measure the actual difference of depolarization between the [111]- and [100]-cut rods, two relative experiments were carried out. The experimental setup is shown in Fig. 5, both of the Nd:YAG rods are 3 mm in diameter and 80-mm long and the doping concentration is 1.0±0.1 at.%. The pump power is up to 180 W by three diode bars. The oscillator configuration is symmetric plane-plane cavity with a cavity length of 245 mm.

The first experiment is to measure the output power of the [111]-cut rod in the steady-state oscillation as the Fig. 5(a). Firstly, we measured the output power without an intracavity Brewster plate polarizer. Then, a polarizer inserted into the cavity to measure the linearly polarized output power as shown in Fig. 5(b). The linearly polarized output power does not depend on the polarization direction. The measured output power in the oscillation is shown in Fig. 6. It can be seen that the linearly polarized output power is obviously smaller than the unpolarized output power due to the depolarization.

The second experiment is to measure the output power of the [100]-cut rod in the steady-state oscillation as the Fig. 5(a). Firstly, we measured the output power without an intracavity Brewster plate polarizer. The curves of the pump power versus the unpolarized output power are quite similar for the [111]- and [100]-cut rods in Fig. 6. The difference is due to the inaccuracy of the Nd:YAG crystal doping concentration. Then, a polarizer inserted into the cavity to measure the linearly polarized output power as the Fig. 6. The linearly polarized output power changed as we rotated the polarizer. The maximum and the minimum linearly polarized output power could be found through suitable modification of the polarization direction. As is evident from the Fig. 6, the minimum linearly polarized output power of the [100]-cut rod is considerably smaller than the value of the [111]-cut rod, but the maximum linearly polarized output power is larger than the value of the [111]-cut rod.

In order to find out the relationship between the linearly polarized output power and the polarization direction in the [100]-cut rod, we rotated the polarizer to align the polarization direction and measured the output power for different polarization directions versus the pump power in Fig. 7. The linearly polarized output power increases while the polarization angle γ changes from 0 to $\pi/4$. The linearly polarized output power reaches a maximum value at the polarization angle of $\gamma = \pi/4$, and it is much higher than that of the [111]-cut rod. It indicates that the depolarization of [100]-cut rod depends on the orientation of the linearly polarized laser with respect to the crystal orientation.

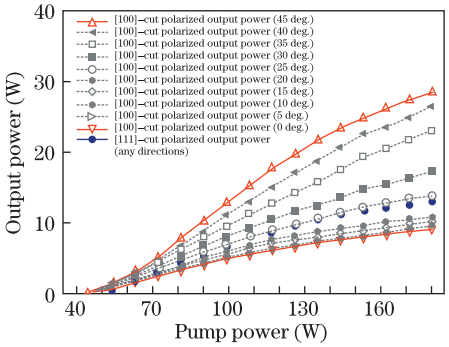

Fig. 7. Measured output power in different polarization directions of [100]-cut Nd:YAG rod with different pump powers.

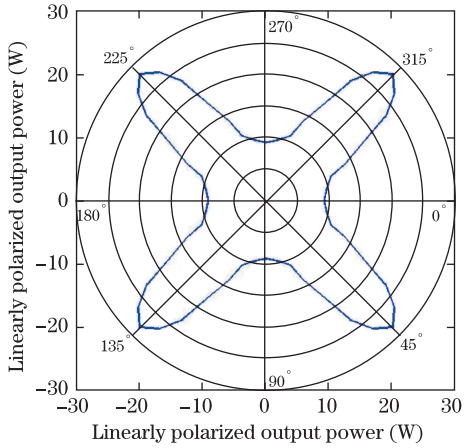

Fig. 8. Measured linearly polarized output power of the [100]-cut rod versus polarization directions at a pump power of 180 W.

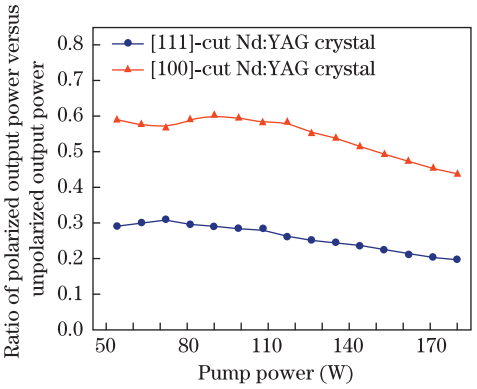

Fig. 9. Ratio of linearly polarized output power versus unpolarized output power achieved with the [111]- and [100]-cut Nd:YAG rods at different pump powers.

We compared the linearly polarized output power for the [111]- and [100]-cut rods. It can be found that the maximum linearly polarized output power from the [100]-cut rod with the polarization angle $\gamma = \pi/4$ is about 3.1 times of the minimum linearly polarized output power of the [100]-cut rod with the polarization angle γ =0 and $\pi/2$. The maximum linearly polarized output power of the [100]-cut rod with the polarization angle $\gamma = \pi/4$ is about 2.2 times of that of the [111]-cut rod with various polarization angles. The experiment results are in good agreement with the theoretical analysis of [111]- and [100]-cut rods.

Figure 8 better reveals the relationship between the linearly polarized output power of the [100]-cut rod and the polarization direction as we rotated the polarizer from 0 to 2π. The curve represents the linearly polarized output power with a pump power of 180 W. As we can see, four maximum values and four minimum values of the polarized output power appear while the polarization angle γ with respect to the crystal orientation changes from 0 to 2π, indicating a period of $\pi/2$.

To further reveal the difference between the depolarization of the two rods, the ratio of the linearly polar-

ized output power versus the unpolarized output power achieves with the two rods are compared with each other in Fig. 9. The difference of depolarization keeps more than 20% at different pump power. At a pump power of 180 W, the ratio of the linearly polarized output power versus the unpolarized output power obtained for the [111]- and [100]-cut rods are 19% and 43% respectively, with a difference of 24%. As the Fig. 9 shows, the ratio of the linearly polarized output power versus the unpolarized output power is steady decrease. It is due to the increase of depolarization loss when increasing the pump power for the [111]- and [100]-cut rods in Eq.(7), the linearly polarized output power versus pump power increase slowly. And the unpolarized output power increases linearly when increasing the pump power in the steady-state oscillation for the both rods.

In conclusion, we have experimentally compared the output power for [111]- and [100]-cut Nd:YAG rods. The maximum linearly polarized output power of the [100]-cut rod is about 2.2 times of that of the [111]-cut rod. For the [100]-cut rod, the maximum linearly polarized output power is about 3.1 times of the minimum linearly polarized output power. These results basically match with theoretical analysis of thermal depolarization. Compared with the [111]-cut rod, the ratio of the linearly polarized output power versus the unpolarized output power obtained with the [100]-cut rod can be improved by more than 20%. The [100]-cut Nd:YAG rod can be used to improve the linearly polarized output power without additional loss and more complex design compared with the conventional [111]-cut rod.

References

1. W. Koechner, *Solid-State Laser Engineering* (Springer, Berlin, 2003).
2. I. Mukhin, O. Palashov, and E. Khazanov, Opt. Express **17,** 5496 (2009).
3. S. D. Jackson and J. A. Piper, Appl. Opt. **35,** 1409 (1996).
4. M. Schmid, R. Weber, T. Graf, M. Roos, and H. P. Weber, IEEE J. Quantum Eelectron. **36,** 620 (2000).
5. M. P. Murdough and C. A. Denman, Appl. Opt. **35**, 5925 (1996).
6. J. Sherman, Appl. Opt. **37,** 7789 (1998).
7. E. A. Khazanov, Quantum Electron. **31,** 351 (2001).
8. W. C. Scott and M. de. Wit, Appl. Phys. Lett. **18,** 3 (1971).
9. J. Richards, Appl. Opt. **26,** 2514 (1987).
10. W. A. Clarkson, N. S. Felgate, and D. C. Hanna, Opt. Lett. **24,** 820 (1999).
11. R. Fluck, M. R. Hermann, and L. A. Hackel, Appl. Phys. Lett. **76,** 1513 (2000).
12. J. J. Morehead, IEEE J. Sel. Top. Quantum Electron. **13,** 498 (2007).
13. L. N. Soms, A. A. Tarasov, and V. V. Shashkin, Sov. J. Quantum Electron. **10,** 350 (1980).
14. I. Shoji and T. Taira, Appl. Phys. Lett. **80,** 3048 (2002).
15. W. Koechner and D. K. Rice, IEEE J. Quantum Electron. **QE-6,** 557 (1970).
16. S. Z. Kurtev, O. E. Denchev, and S. D. Savov, Appl. Opt. **32,** 278 (1993).
17. I. B. Mukhin, O. V. Palashov, E. A. Khazanov, and I. A. Ivanov, JETP Lett. **81,** 90 (2005).
18. O. Puncken, H. Tünnermann, J. Morehead, P. Weßels, M. Frede, J. Neumann, and D. Kracht, Opt. Express **18,** 20461 (2010).
19. H. Tünnermann, O. Puncken, P. Weßels, M. Frede, J. Neumann, and D. Kracht, Opt. Express **19,** 12992 (2011).